J. Fluid Mech. (2014), *vol.* 750, *pp.* 385–400.
doi:10.1017/jfm.2014.288

Dynamic transition from Mach to regular reflection of shock waves in a steady flow

K. Naidoo[1] **and B. W. Skews**[2,†]

[1]DPSS, Council for Scientific and Industrial Research, PO Box 395, Pretoria 0001, South Africa

[2]Flow Research Unit, School of Mechanical, Industrial and Aeronautical Engineering, University of the Witwatersrand, Johannesburg 2050, South Africa

(Received 7 November 2013; revised 29 April 2014; accepted 20 May 2014; first published online 9 June 2014)

The steady, two-dimensional transition criteria between regular and Mach reflection are well established. Little has been done on the dynamic effect on transition due to a rapidly rotating wedge. Results from experiments and computations done on steady and unsteady shock wave transition from Mach reflection to regular reflection, MR $\rightarrow$ RR, are described. The measured motion and the initial shock incidence was used to mimic the experiment with a two-dimensional numerical code. The maximum rotation speed achieved at transition was approximately 2500° s^{-1}. Rapid wedge rotation was shown to have a significant measurable effect on transition. The code was also applied to the dependence of dynamic MR $\rightarrow$ RR transition on other variables in the parameter space. These include rotation about the leading or trailing edge, initial incidence and rotation speed at two free-stream conditions. Impulsively started rotation in these cases was used with the rotation specified by $M_E = \omega c/a_\infty$ where ω is constant angular velocity (negative anticlockwise), c the distance from the edge considered to the pivot point and a_∞ the free-stream sound speed. For the Mach numbers and range of rotation speeds tested, both the wedge and shock angle at transition decreased with increased rotation speed. The sensitivity of the transition angle to changing the rotation point from the trailing edge to the experimental model pivot point was investigated briefly at a free-stream Mach number of $M = 2.98$ with $M_E = -0.1$. The wedge angle at transition increased by 1.5° and the shock angle at transition decreased by 1.5°, a significant variation. The effect of the initial incidence was also investigated. By reducing the initial wedge angle from 24.5 to 23.5° for these initial conditions the shock angle at transition decreased by approximately 1.8°, also a marked sensitivity. The flow field development for impulsive rotation about the wedge trailing and leading edges at $M = 1.93$ for $M_E = -0.075$ was analysed in some detail. The flow field development is very sensitive to the rotation centre, more especially at large rotation rates. Four phases of the Mach stem development were identified in both cases. For rotation about the wedge leading edge the Mach stem height remains constant until the expansion waves arrive at the triple point. This is followed by an increase in Mach stem height, which then remains constant for a short period after which it decreases until transition to RR. For rotation about the wedge trailing edge the impulsive start generates a disturbance on the incident wave which propagates down the wave, through the triple point and down the Mach stem. The stem height is constant until the arrival of the incident wave disturbance. This causes a sudden decrease in Mach stem height. Subsequently, the Mach stem height

† Email address for correspondence: beric.skews@wits.ac.za

remains constant for a short time, before it decreases until transition to RR. Similar effects in the variation of stem height with wedge angle occur at the higher Mach number of 2.98. It was demonstrated that MR can be maintained for a while at zero wedge incidence with a sufficiently large rotation rate of $M_E = -0.1$, with $M = 1.93$, for both leading and trailing edge pivot points.

Key words: compressible flows, gas dynamics, shock waves

1. Introduction

When a plane shock wave from a wedge in a steady supersonic flow strikes a surface, two reflection patterns are commonly observed, as sketched in figure 1. The incident wave, I, starting from the wedge tip results in a reflected wave, R. In the Mach reflection case they meet at the triple point, T, with the Mach stem, H of height m, between it and the surface. A slipstream, S, propagates away from this three-shock intersection. An expansion wave, E, originates at the trailing edge of the wedge. The nomenclature for angles between the various features and the relevant dimensions are given in the sketch. The transition between them, as the wedge angle is changed, is well documented (Ben-Dor 2007), with the theoretical boundaries shown and labeled in figure 2. Below a free-stream Mach number of 2.202 ($\gamma = 1.4$), in the so-called weak reflection regime, there is a single boundary between them, the detachment condition, but for strong shocks a second boundary, the von Neumann condition, appears. Between this and the detachment condition both regular and Mach reflection are possible and transition occurs depending on whether the shock, and wedge angle, are increasing or decreasing.

There have been limited studies as to what happens with rapid wedge rotation since there are time delays between a change of wedge angle and the influence on the reflection plane because of the finite propagation speed of disturbances. A recent study by the authors (Naidoo & Skews 2011) showed that there are considerable differences in the transition conditions if the wedge is rotated rapidly. That paper should be consulted for more details of the theoretical and historical background to these studies. It also details the experimental and numerical arrangements used. The same equipment and facilities were used as in the current study and that paper should be consulted if such background to the current study is required.

The main emphasis in that earlier study was the transition from regular to Mach reflection, and further details on the flow mechanisms causing the differences between steady and unsteady transition conditions for the RR $\rightarrow$ MR transition has recently been added (Naidoo & Skews 2013), dealing with the case of increasing wedge incidence. It was found in some cases in the weak reflection regime, and depending on the rotation rate, transition can occur before information from the wedge trailing edge reaches the reflection point, i.e. there is no length-scale condition. For some cases in the strong reflection regime the length-scale information reaches the reflection point but transition occurs somewhat later, so again the steady-state length-scale criterion also does not apply. Reasons for this behaviour are discussed in the above paper, relating to the transient propagation of information from the wedge surface.

The current study examines the reverse transition from Mach to regular reflection, MR $\rightarrow$ RR, which is somewhat more complex. This complexity arises because of the expansion or compression waves arising from the wedge motion, which depend on

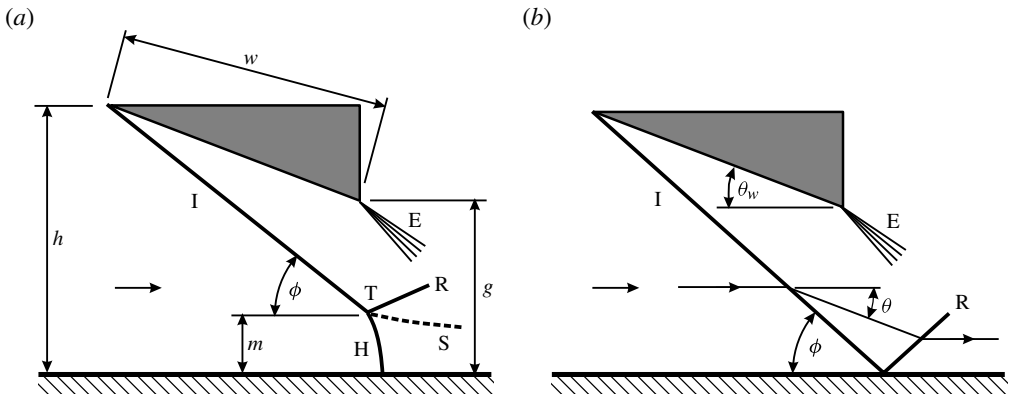

FIGURE 1. Simplified schematics of Mach and regular reflection generated by a wedge in a steady supersonic free stream.

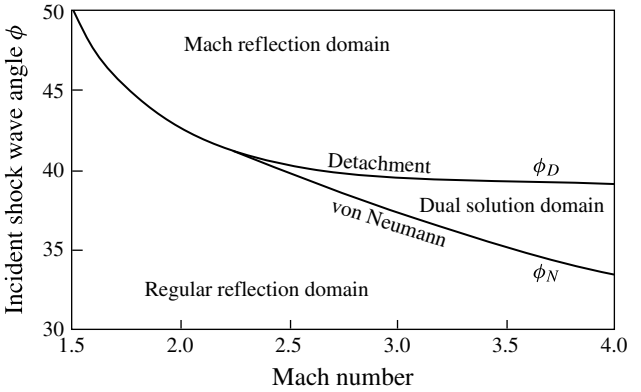

FIGURE 2. Domains of shock reflection.

whether the pivot point is at the leading or trailing edge, taking time to arrive at the triple point, then propagating down the Mach stem until arriving at the reflection plane causing adjustments there.

2. Method

2.1. *Experiments*

A pair of wedges of 40 mm chord and 170 mm span were placed symmetrically in the wind tunnel with the plane of symmetry between them acting as the rigid ground plane, being inviscid, impermeable and adiabatic. The supersonic wind tunnel at the CSIR, South Africa, has a 450 mm $\times$ 450 mm test cross-section. Further details of the experimental set-up are described in Naidoo & Skews (2011). Flow visualisation was achieved with a standard z-configuration schlieren system. Imaging was done with a Photron Ultima APX-RS high-speed camera at 250 f s^{-1} (1024×1024 pixel resolution) for the steady-state tests and at 10 000 f s^{-1} (512×512 pixel resolution) for the dynamic tests.

Accurate measurement of θ_w, ϕ and Mach stem height m, from images is important to this investigation. The calibration of the schlieren optics for coordinate and

Data point	Calculated angle 10.0°	Error	Calculated angle −10.0°	Error
1	9.930	0.070	−10.076	0.076
2	9.800	0.200	−10.283	0.283
3	9.892	0.108	−10.283	0.283
4	10.001	−0.001	−10.222	0.222
5	9.921	0.079	−10.143	0.143

TABLE 1. Example results from a calibration check on a test image for measurements at 10.0 and −10.0°.

Mean error	0.035°
Standard deviation	0.155°
Maximum error	0.316°
95 percentile	0.28°

TABLE 2. Summary of statistics for angular measurement error.

angular measurements involved imaging a 5 mm × 5 mm uniform grid and a test pattern consisting of lines at known angular orientations, placed on the test section window and thereafter transforming from the coordinate system imaged to the object coordinate system. Pixel coordinates of 10 points along lines of interest were transformed to object space coordinates to calculate the orientation of each line with a linear regression of the measured points, to compare with the known accurate grid values. Typical results of a calibration check for a few cases are given in table 1. A summary of statistics on the measurements are listed in table 2. From these the uncertainty in angular measurement is estimated at approximately ±0.3°, a value slightly larger than the 95 percentile of the calculated errors.

The uncertainty of distance measurement was estimated by measuring the distance between the ends of any two lines bounding a five degree arc on the test image and comparing the result with the true value (approximately 4.362 mm). Results are presented in table 3. The maximum error was approximately 0.08 mm. This translates to a measurement uncertainty on m/w of approximately 0.002. This does not necessarily account completely for the uncertainty in locating the triple point on an image of a MR. By considering images of a MR, the uncertainty in the non-dimensional Mach stem height measurement is estimated at approximately 0.4 % of the wedge chord.

The wedges were rotated gradually between 5.0 and 10° s^{-1} to generate steady-state data. They were rotated at larger speeds with a spring-driven actuator for the dynamic case. The drive train is accelerated at approximately 1000 m s^{-2} over a period of approximately 6.0 ms. The wedge pivot point was positioned as close to the trailing edge as possible. The exact location is specified in figure 9 of Naidoo & Skews (2011) together with a more comprehensive description of the experimental facility. The vertical movement of the trailing edge between the wedge incidence $\theta_w = 2.0°$ and $\theta_w = 25.0°$ is approximately 2.1 % of the wedge chord.

2.2. *Computation*

An in-house Euler code specifically developed for moving boundary problems such as the current case (Felthun & Skews 2004) was used. Beside mimicking the experiment,

Data point	Measured distance	Error (mm)
1	4.426	0.064
2	4.442	0.080
3	4.301	0.061
4	4.417	0.055
5	4.297	0.065
6	4.422	0.060
7	4.435	0.073
8	4.305	0.057

TABLE 3. Calibration check for measurement uncertainty on distance.

	$M = 1.93$ (deg.)	$M = 2.98$
Analytical, ϕ_T	43.2	$\phi_N = 37.5°$ $\phi_D = 39.5°$
2D Euler CFD, ϕ_T	43.4	MR $\rightarrow$ RR 37.5°
Experiment, ϕ_T	43.4	37.4°

TABLE 4. Summary of steady state results at $M = 1.93$ and 2.98, $g/w \approx 0.6$.

use was extended to investigate the effect of the pivot point, initial incidence and rotation speed on the dynamic transition. Details of the code and its validation are given in Naidoo & Skews (2011). The simulations conducted for comparison with experiment used identical geometry to that of the experiment including the position of the pivot point.

3. Experiments in dynamic transition from Mach to regular reflection

3.1. *Steady-state tests*

Steady-state tests were conducted to generate a baseline against which the dynamic tests could be compared. Additional complexities arise because starting with a Mach reflection, the flow behind the Mach stem is subsonic and therefore peripheral edge effects can propagate into the region behind it. Thus three-dimensional influences could influence the reflection pattern in the streamwise vertical plane of symmetry (Skews 2000). Two- and three-dimensional computational and experimental data by Ivanov *et al.* (2001), showed that the Mach stem height is influenced by three-dimensional effects and is smaller than the two-dimensional result. However, the shock angle at transition, ϕ_T, approaches the same value for the two cases and corresponds to the theoretical value. This was confirmed by Naidoo & Skews (2011) as shown in table 4.

3.2. *Experiments*

Owing to the way in which the tunnel flow starts and the current rig geometry, the flow sets up an initial detached wave system with a normal shock spanning the wedges at the inlet. It was not found possible to set up an initial, steady MR in the weak-reflection range, since as the wedge angle was decreased the normal shock at the inlet is swallowed and settles as a steady regular reflection. The Mach reflection pattern is transient. Reversing the wedge motion results in the shock becoming detached, without passing through a steady Mach reflection state. Further studies are

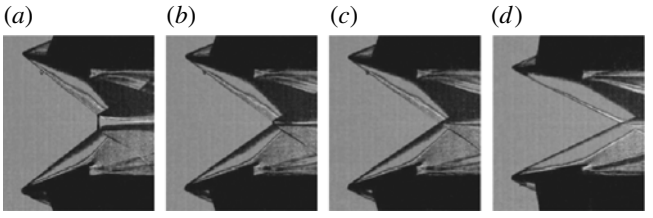

FIGURE 3. Schlieren images of MR → RR for $M = 3.26$: (*a*) $t = 1.1$ ms, $\theta_w = 21.4°$, $\phi = 39.0°$; (*b*) $t = 2.4$ ms, $\theta_w = 18.9°$, $\phi = 36.4°$; (*c*) $t = 2.7$ ms, $\theta_w = 18.2°$, $\phi = 35.5°$; (*d*) $t = 5.2$ ms, $\theta_w = 9.2°$, $\phi = 26.2°$.

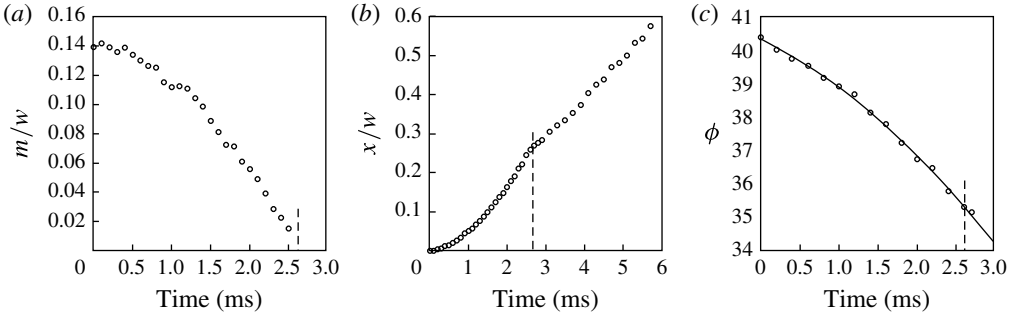

FIGURE 4. Measurements from the dynamic experiment at $M = 3.26$. The time of MR → RR transition is estimated from the images and is indicated on each graph with a broken line.

required to examine these effects. Experiments for dynamic MR → RR transition were done at $M = 3.26$ and 2.96. In both experiments, an initial steady MR is set up followed by the rapid decrease in wedge incidence until transition to RR. In both experiments RR persisted below ϕ_{NC}. The additional C subscript refers to a corrected theoretical von Neumann value based not just on the tunnel free-stream Mach number but accounting for the motion of the reflection point on the symmetry plane relative to the free stream at transition, resulting in a slight adjustment to the Mach number. Owing to the similarity in the results for the two Mach numbers only the case $M = 3.26$ will be discussed. Selected high-speed images for the experiment are given in figure 3. Zero time corresponds to the image frame just before any wedge movement is visible on the high-speed images. In the final image the reflection pattern is clearly RR.

Measurements from the images are included in figure 4, i.e. time histories of Mach stem height, the streamwise location of the reflection/triple point, and shock incidence. The zero reference for the streamwise location is the position of the stem during the steady-state start before the wedge starts rotating. After tunnel startup, an initial, steady MR is set up just beyond the dual solution domain, with $\theta_w = \theta wi$, after which time the wedge incidence was reduced rapidly. As θ_w decreases, the Mach stem moves downstream and the Mach stem height decreases until transition to RR. The position of transition obtained from the height information is marked on all plots. The wedge rotation continues well after transition, but the flow field after transition is not analysed further. The instantaneous rotation speed at the point of transition was approximately 2500° s^{-1} with $M_E = -0.008$, approximately 0.8 % of

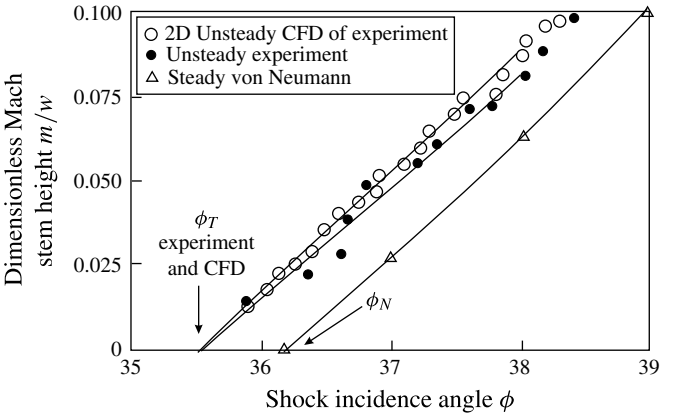

FIGURE 5. Mach stem development from experiment and CFD for dynamic MR → RR transition at $M = 3.26$, $g/w \approx 0.6$.

Analytical steady von Neumann condition, ϕ_N	36.2°
Measured relative Mach number of reflection point at transition	−0.03
Corrected analytical steady von Neumann condition ϕ_{NC}	36.3°
Experiment: dynamic ϕ_T	35.5°
2D Euler CFD: steady-state ϕ_T	36.2°
2D Euler CFD: dynamic ϕ_T	35.5°
Difference between dynamic ϕ_T and ϕ_{NC} (CFD and experiment)	≈0.8°

TABLE 5. Experimental and CFD results for steady and dynamic MR → RR transition at $M = 3.26$, $g/w \approx 0.6$.

the free-stream acoustic speed. The tunnel conditions, measured wedge motion and initial shock angle, ϕ_i were used as inputs to the CFD simulation. Since the Euler equations do not model the flow deflection due to the wedge surface boundary layer, θ_i in the simulation was corrected to achieve the same ϕ_i in the experiment.

The experimental and computed Mach stem height variation with shock incidence angle is presented in figure 5. A linear fit to both data sets, only for $\phi \leqslant 38.0$, is used to extrapolate ϕ_T at zero m/w. The expected, initial difference in Mach stem height between the CFD and experiment is small at the initial condition, θ_{wi}, but as the wedge rotates there is a deviation from the steady case. As the Mach stem height decreases, the unsteady CFD and experiment converge to $\phi_T \approx 35.5$, although the scatter in the experimental data means the experimental transition is less certain. The analytical transition condition was corrected for the speed of the triple point at transition and results are summarised in table 5. Transition was observed approximately 0.8° below ϕ_{NC} and there is close agreement on ϕ_T between the experiment and computation. Although the rotation speeds achieved here were not as large as in the RR → MR transition experiments, the dynamic effect of rapid wedge rotation on ϕ_T is still evident.

The Mach stem development from a simulation with the same free-stream condition and ϕ_i, but with a larger and constant rotation speed about the wedge trailing edge at $M_E = -0.05$, shows even more deviation from the steady case. Transition to RR was predicted at $\phi_T \approx 32.76°$, 3.5° below ϕ_N and 4.5° below ϕ_{NC}

Analytical steady von Neumann condition, ϕ_N	37.6°
Measured relative Mach number of reflection point at transition	−0.02
Corrected analytical steady von Neumann condition ϕ_{NC}	37.6°
Experiment: dynamic ϕ_T	37.0°
2D Euler CFD: dynamic ϕ_T	36.8°
Difference between dynamic ϕ_T and ϕ_{NC} (CFD and experiment)	≈0.6–0.8°

TABLE 6. Experimental and CFD results for steady and dynamic MR → RR transition at $M = 2.96$, $g/w \approx 0.6$.

A similar result was observed at $M = 2.96$. Transition results are summarised in table 6. Transition was observed approximately 0.6–0.8° below ϕ_{NC}. Once again, there is close agreement between the experiment and 2D Euler CFD result.

4. Impulsive start

Having established the necessary confidence in the Euler code to adequately model the dynamic flow field of interest, this section explores the sensitivity of ϕ_T as well as the dynamic flow field development to rotation speed and pivot point at $M = 1.93$ and 2.98 with CFD simulations. The sensitivity of ϕ_T to θ_{wi} is also investigated briefly. The wedge is rotated a constant angular speed, i.e. fixed M_E following an impulsive start. This initial condition helps in the interpretation of the flow physics and the effects of unsteadiness.

When θ_w is decreased *gradually* from an initial, steady MR such that the flow field is approximately steady state at each point in time, the Mach stem decreases continuously with a decrease in θ_w until transition to RR. Transition occurs at the detachment condition, with $\phi_T = \phi_D$ in the weak-reflection region and at the von Neumann condition, with $\phi_T = \phi_N$, in the strong-reflection region. MR → RR transition occurs when the triple point reaches the reflection plane. Transition is dependent on the initial Mach stem height, which is dependent on the free-stream condition, ϕ_i and g/w or h/w. The theoretical transition angles are recalculated to take into account the decrease in local Mach number at the triple point due to its streamwise movement. The corrected wedge and shock incidence at the detachment and von Neumann conditions are labeled θ_{DC}, ϕ_{DC} and θ_{NC}, ϕ_{NC}, respectively. The abbreviations TE (wedge trailing edge) and LE (wedge leading edge) will be appended to labels of quantities to indicate the rotation centre.

4.1. *Weak reflection regime*

An initial, steady MR is set up at $\theta_{wi} = 13.4°$ in a $M = 1.93$ free stream with $h/w = 0.84$. The wedge is started impulsively and, for the first tests, rotated about its leading edge with $M_E = -0.075$ until $\theta_w = 0°$. The Mach stem evolution with respect to θ_w and ϕ is shown in figure 6. Four phases of the triple point movement are identified. Computed pressure contours showing the development of the flow field are presented in figures 7 and 8.

Phase I: As the wedge rotates about its leading edge, with the trailing edge moving away from the reflection plane, expansion waves are generated from the surface and propagate toward the triple point, figure 7(*a*). Due to the rapid rotation speed, the wedge rotates some 1.9° before the surface expansion reaches the triple point. Up to this time the triple point is unaware of the wedge movement and the Mach stem height

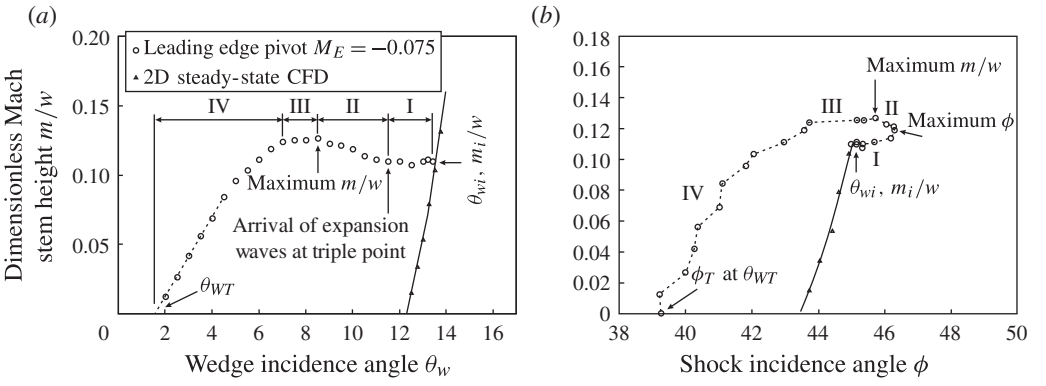

FIGURE 6. Computed variation of m/w with θ_w and ϕ for impulsive rotation about the leading edge at $M_E = -0.075$, $M = 1.93$, $\theta_{wi} = 13.4$ and $h/w = 0.84$.

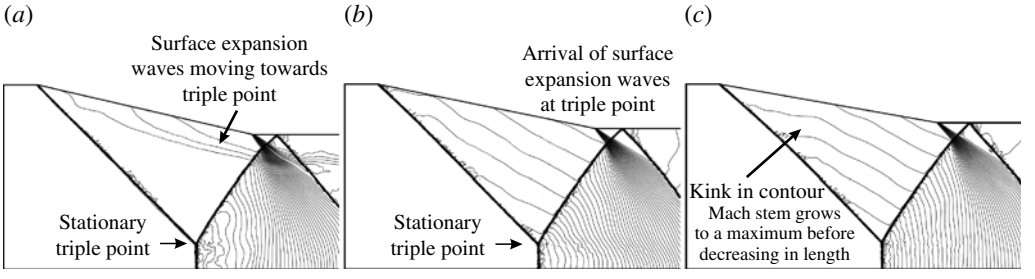

FIGURE 7. Pressure contours for early flow development following impulsive start about the leading edge, $\theta_{wi} = 13.4°$, $M_E = -0.075$, $M = 1.93$, $h/w = 0.84$: (*a*) $\theta_w = 13.0°$, $t = 14.1$ μs, phase I; (*b*) $\theta_w = 11.5°$, $t = 67$ μs, phase I/II boundary; and (*c*) $\theta_w = 10.0°$, $t = 119.9$ μs, phase II.

is constant. The kink in the pressure contours in figure 7(*c*) clearly shows the change in the expansion waves resulting from the impulsive start to those resulting from the uniform rotation. In the experiment these would be curved due to the changing acceleration.

Phase II: When the expansion waves reach the triple point at $\theta_w = 11.5°$, the expansion has the effect of sucking the triple point away from the reflection plane and increasing the Mach stem height. This effect was first observed and discussed briefly in Felthun & Skews (2004) for rapid, impulsive rotation about the wedge leading edge at $M = 3.0$. The Mach stem height increases until the end of phase II at $\theta_w = 8.5°$.

Phase III: Between $\theta_w = 8.5$ and $7.0°$, there is very little change in Mach stem height. The reason for this is not clear.

Phase IV: The Mach stem height decreases until transition to RR at $\theta_{WT} = 1.7$ (figure 8). The wedge incidence at transition is estimated with a linear extrapolation of the data for $\theta_w \leqslant 4.5°$. At transition to RR, a normal shock is generated developing a pattern similar to transitioned regular reflection (TRR) of a plane shock off a curved surface.

Consider the variation of m/w with ϕ in figure 6. The data points are connected with a dashed line to clarify the sequence of events. Results for the steady, 2D

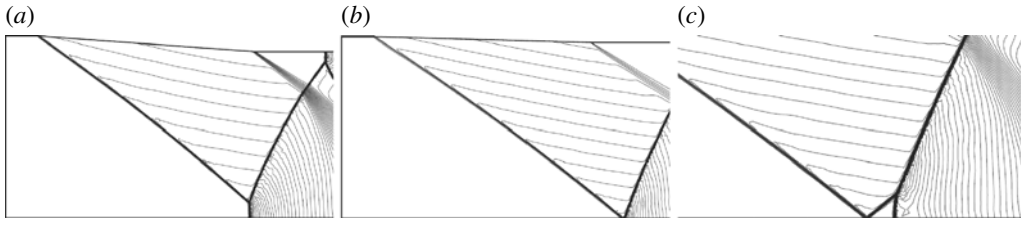

FIGURE 8. Pressure contours for late flow development following impulsive start about the leading edge, phase IV, $\theta_{wi} = 13.4°$, $M_E = -0.075$, $M = 1.93$, $h/w = 0.84$: (*a*) $\theta_w = 4.0°$, $t = 331.4$ μs; (*b*) $\theta_w = 1.5°$, $t = 419.6$ μs; and (*c*) $\theta_w = 0.5°$, $t = 454.8$ μs (enlarged view).

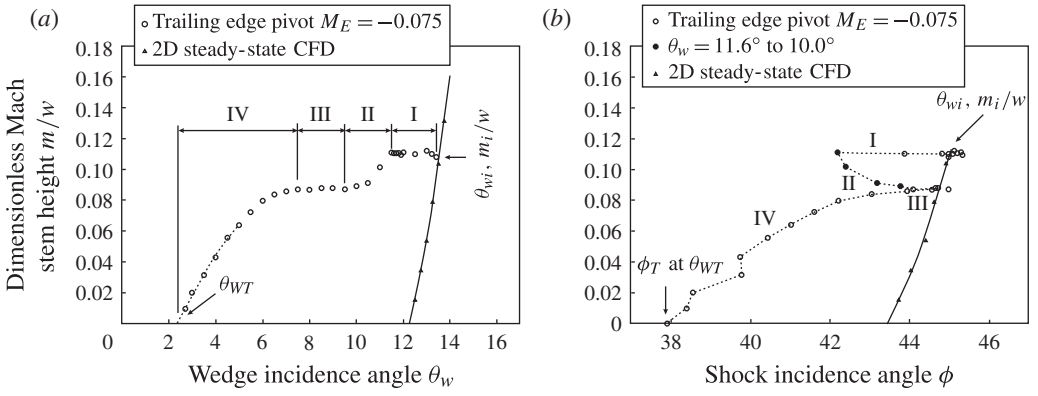

FIGURE 9. Computed variation of m/w with θ_w and ϕ for impulsive rotation about the trailing edge at $M_E = -0.075$, $M = 1.93$, $\theta_{wi} = 13.4°$ and $g/w = 0.6$.

computation are superimposed. The shock incidence and Mach stem height remain unchanged at $\phi = \phi_i = 45.1°$ and $m/w = m_i/w = 0.11$ in phase I, where m_i is the initial steady Mach stem height. As the triple point moves away from the reflection plane, the suction has the effect of increasing the shock incidence to a maximum value of $\phi = 46.3°$ at the triple point. The point of maximum shock incidence does not coincide with the point of maximum Mach stem height. Before the maximum Mach stem height is achieved the shock incidence decreases and continues to do so until transition with $\phi_T \approx 39.2°$.

The flow is somewhat different for rotation about the trailing edge. Similar boundary conditions are applied with an initial, steady MR set up at $\theta_{wi} = 13.4°$ in a $M = 1.93$ free stream and $M_E = -0.075$ but now with a fixed trailing edge position of $g/w = 0.6$. The variation of m/w with θ_w and ϕ is given in figure 9. Figures 10 and 11 show a selection of pressure contours from the CFD simulation between $\theta_w = 13.0°$ and $\theta_w = 1.1$. Four phases of the triple point movement are again identified.

Phase I: The impulsive movement of the wedge tip generates a disturbance on the incident wave that propagates at a speed equal to the sum of the local acoustic speed and the local velocity component parallel to the wave until they reach the triple point. The dashed grey lines in figures 10 and 11 correspond to the planar incident wave at the initial condition and is shown to highlight the propagation of the disturbance on the incident wave. There cannot be any movement of the incident wave downstream of the disturbance. In phase I, figure 10(*a*), the triple point is unaware of the movement

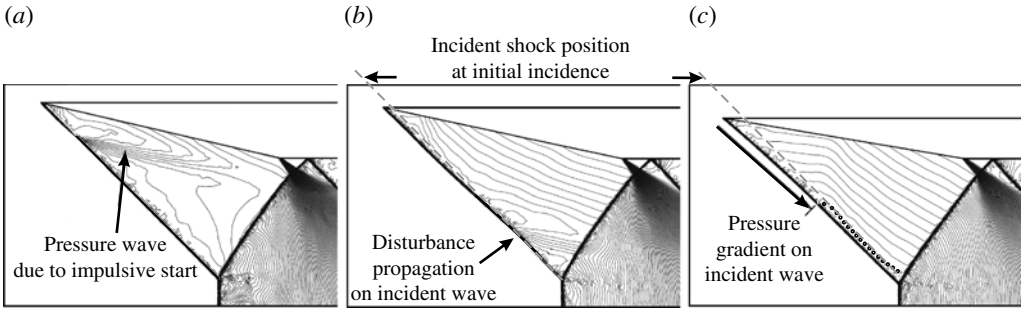

FIGURE 10. Pressure contours for early flow development following impulsive start about the trailing edge, $\theta_{wi} = 13.4°$, $M_E = -0.075$, $M = 1.93$, $g/w = 0.6$: (*a*) $\theta_w = 13.0°$, $t = 14.1$ μs, phase I; (*b*) $\theta_w = 12.0°$, $t = 49.4$ μs, phase I/II boundary; and (*c*) $\theta_w = 9.5°$, $t = 137.5$ μs, phase II.

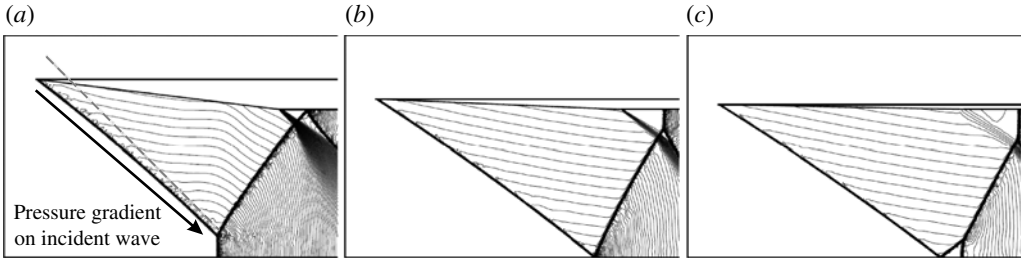

FIGURE 11. Pressure contours for late flow development following impulsive start about the trailing edge, phase IV, $\theta_{wi} = 13.4°$, $M_E = -0.075$, $M = 1.93$, $g/w = 0.6$: (*a*) $\theta_w = 7.0°$, $t = 225.6$ μs; (*b*) $\theta_w = 2.4°$, $t = 387.8$ μs; and (*c*) $\theta_w = 1.1°$, $t = 433.7$ μs.

of the wedge and the Mach stem height is constant until the disturbance reaches the triple point at $\theta_w \approx 11.6°$.

Phase II: For $\theta_w = 11.6°$ to $\theta_w = 10.0°$ the disturbance travels from the triple point and down the Mach stem, toward the reflection plane. As the disturbance passes down through the Mach stem its height decreases rapidly and then more slowly until $\theta_w = 9.5°$.

Phase III: Between $\theta_w = 9.5$ and $7.5°$, the disturbance has already passed through the triple point and there is little further change in Mach stem height until the start of phase IV at $\theta_w = 7.5°$.

Phase IV: After phase III the Mach stem height decreases until transition at $\theta_{WT} = 2.4°$.

The underlying phenomena that result in phases III and IV are not clear. Consider the pressure contours in figure 10(*c*). The pressure contour between the incident and reflected waves that is closest to the triple point, is highlighted by a series of small circles. The intersection of this isobar with the incident wave indicates a discontinuity in curvature on the incident wave. The incident wave upstream of the discontinuity is curved and there is a pressure gradient along this segment. There is no pressure gradient along the planar segment downstream of the discontinuity. As θ_w decreases the discontinuity moves toward the triple point. By $\theta_w = 7.5°$ the incident wave is curved along its entire length. It appears that the start of phase IV in which the Mach stem height decreases, is coincident with the arrival of the discontinuity on the

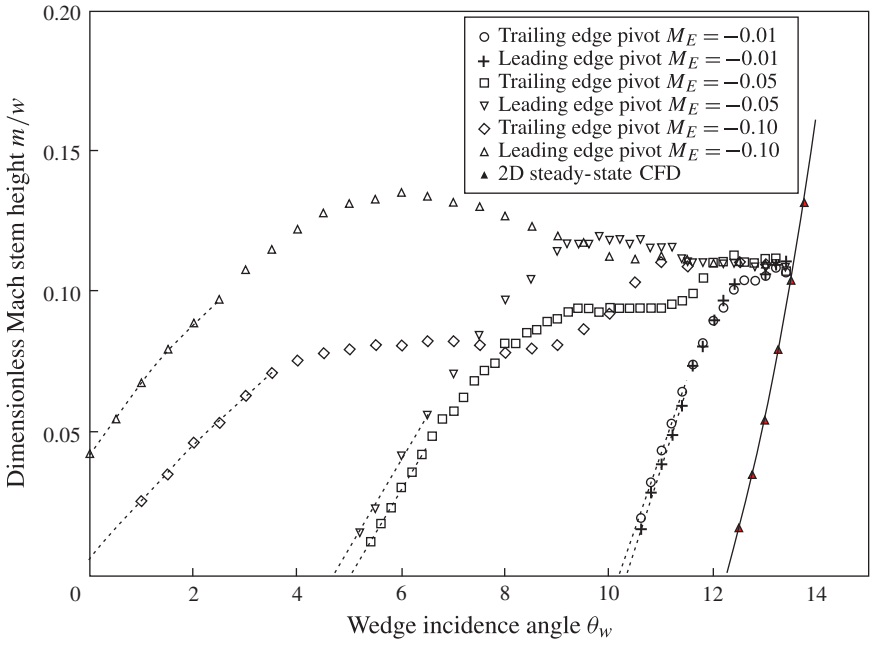

FIGURE 12. Computed variation of m/w with θ_w for rapid, impulsive rotation about the wedge leading and trailing edges with fixed $h/w = 0.84$ (for rotation about the leading edge) and fixed $g/w = 0.6$ (for rotation about the trailing edge). In all cases plotted here, $\theta_{wi} = 13.4°$, $M = 1.93$.

incident wave at the triple point. However, it is not certain if the Mach stem height decreases due to the arrival of the discontinuity.

The variation of m/w with ϕ is given in figure 9. The Mach stem height remains constant until the arrival of the disturbance on the incident wave at the end of phase I. As the disturbance passes through the triple point there is a sudden decrease in m/w and increase of ϕ in phase II. In phase III, ϕ and m/w are essentially constant. In phase IV, ϕ and m/w decrease until transition at $\phi_T = 37.9°$.

Consider the variation of m/w with θ_w in figure 12 (for $M_E = -0.01$, -0.05 and -0.1). The dynamic effect of rapid rotation on the Mach stem development for $M_E = -0.075$ presented earlier are not visible at $M_E = -0.01$. It would appear that at this smaller rotation rate, the rotation centre makes little difference to the transient Mach stem development or to the values of θ_{wT} and ϕ_T. While the Mach stem development at $M_E = -0.01$ is consistent with the observations made at $M_E = -0.075$, the impulsive start and rapid rotation for $M_E = -0.1$ result in a situation in which MR is maintained even at $\theta_w = 0°$. Selected pressure contours for rapid rotation about the leading edge are presented in figure 13. The wedge is started impulsively at $\theta_{wi} = 13.4°$ and stopped at $\theta_w = 0°$. At $\theta_w = 0°$, the wave system detaches from the wedge tip and proceeds to wash downstream. The Mach stem on the residual wave reflection is clearly visible in figure 13(*c*). Figure 14 shows magnified views in the vicinity of the reflection plane showing the transition of the residual reflection from MR to RR as the wave system washes downstream. The incident wave, and then the reflected wave, will eventually vanish. The results are summarised in table 7.

For the range of rotation speeds investigated, where $\delta\theta_{WT}$ and $\delta\phi_T$ increased with an increase in rotation speed, where δ represents the difference between the steady and

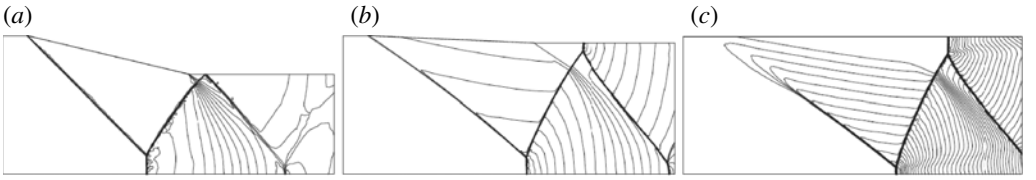

FIGURE 13. Computed pressure contours for impulsive rotation at $M_E = -0.1$, $M = 1.93$, $\theta_{wi} = 13.4°$, $h/w = 0.84$: (*a*) $t = 0$ s, $\theta_{wi} = 13.4°$; (*b*) $t = 10.6$ μs, $\theta_{wi} = 2.5°$; (*c*) $t = 23.8$ μs, $\theta_{wi} = 0°$.

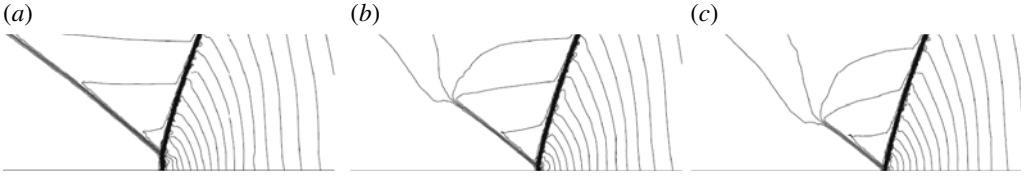

FIGURE 14. Magnified computed pressure contours for impulsive rotation at $M_E = -0.1$, $M = 1.93$, $\theta_{wi} = 13.4°$, $h/w = 0.84$: (*a*) $t = 50.2$ μs, $\theta_{wi} = 0°$; (*b*) $t = 71.4$ μs, $\theta_{wi} = 0°$; (*c*) $t = 76.7$ μs, $\theta_{wi} = 0°$.

M_E	−0.01	−0.05	−0.075
$\theta_{WT,TE}$	10.3	5.2	2.4
$\phi_{T,TE}$	42.1	39.5	37.9
$\theta_{WT,LE}$	10.3	4.9	1.7
$\phi_{T,LE}$	42.0	39.9	39.2

TABLE 7. Wedge and shock incidence at transition: $M = 1.93$, $\theta_{wi} = 13.4°$.

unsteady flow cases. For the range of rotation speeds investigated, $1.2° \leqslant \delta\theta_{T,TE} \leqslant 7.1°$ and $1.0° \leqslant \delta\theta_{T,LE} \leqslant 6.2°$. The corresponding deviation of ϕ_T from ϕ_{DC} ranges as follows: $1.5° \leqslant \delta\phi_{T,TE} \leqslant 7.4°$ and $1.7° \leqslant \delta\phi_{T,LE} \leqslant 7.9°$. In contrast, the maximum deviation observed at $M_E = -0.1$ for RR → MR transition was in the order of $\delta\phi_T = 1.6°$, significantly smaller than the maximum values observed here (Naidoo & Skews 2013).

4.2. *Strong reflection regime*

The variation of m/w with θ_w at $M_E = -0.01$, -0.05 and -0.1 as well as the resultant θ_{WT} and ϕ_T was also investigated at $M = 2.98$. Table 8 summarises values for θ_T and ϕ_T.

Figure 15 gives the data for the effect of θ_w on the Mach stem height. In general, the form of the trend in comparison with the results at $M = 1.93$ is similar. However, a small, but perhaps significant difference, is noted at $M_E = -0.1$ for rotation about the wedge trailing edge. After phase II in which the Mach stem height decreases, there is a small but observable increase in height whereas it is constant in phase III in figure 9. This is also noted at $M_E = -0.05$ for rotation about the wedge trailing edge. Figure 16 gives the corresponding data in terms of the shock wave incidence angle.

For the range of rotation speeds investigated, $\delta\theta_{WT}$ and $\delta\phi_T$ increased with an increase in rotation speed, $1.2° \leqslant \delta\theta_{T,TE} \leqslant 10.4°$ and $1.1° \leqslant \delta\theta_{T,LE} \leqslant 10.0°$. The

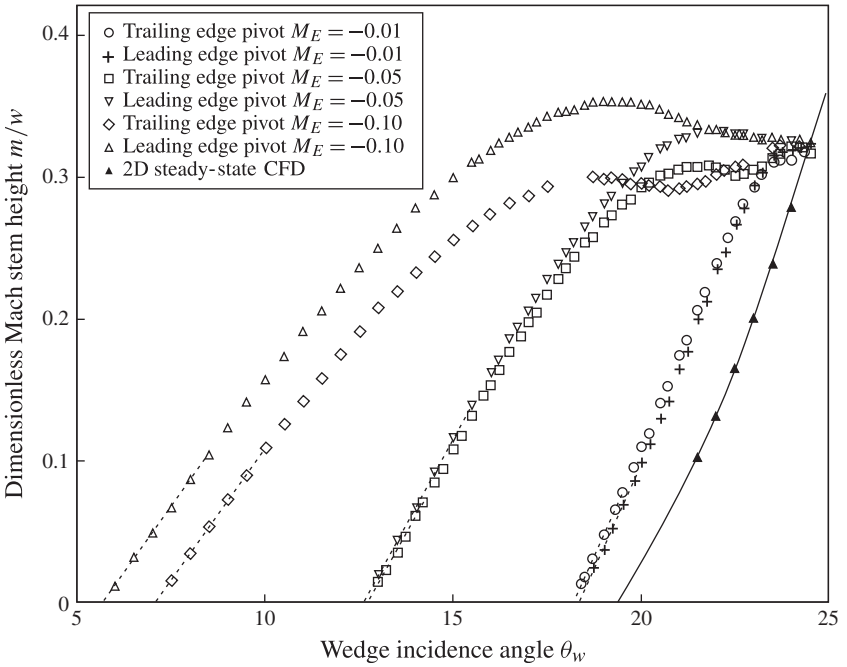

FIGURE 15. Computed variation of m/w with θ_w for rapid, impulsive rotation about the wedge leading and trailing edges with fixed $h/w = 1.01$ (for rotation about the leading edge) and fixed $g/w = 0.6$ (for rotation about the trailing edge). In all cases plotted here, $\theta_{wi} = 24.5°$, $M = 2.98$.

M_E	-0.01	-0.05	-0.1
$\theta_{WT,TE}$	18.2	12.7	7.1
$\phi_{T,TE}$	36.3	32.5	29.0
$\theta_{WT,LE}$	18.3	12.6	5.7
$\phi_{T,LE}$	36.3	32.8	30.2

TABLE 8. Wedge and shock incidence at transition: $M = 2.98$, $\theta_{wi} = 24.5°$.

corresponding deviation of ϕ_T from ϕ_{DC} ranges as follows: $1.5° \leqslant \delta\theta_{T,TE} \leqslant 10.9°$ and $1.5° \leqslant \delta\theta_{T,LE} \leqslant 10.9°$.

The effect of initial incidence and rotation centre were investigated very briefly. Results are summarised in table 9. Results in rows 2 and 3 are compared with the results in row 1. Consider the result in row 2 which shows the sensitivity of transition to changing the pivot point from the trailing edge to the model pivot point in the experiment. Here $\delta\theta$ increases by approximately 1.5° and $\delta\phi$ reduces by approximately 1.5°. This difference is likely to be smaller at a smaller rotation rate. Consider the result in row 3 which shows the sensitivity of transition to reducing the initial incidence. The change in $\delta\theta$ is very small and $\delta\phi$ reduces by approximately 1.8°. Owing to the complex nature of the dynamic case, it is not possible to generalise the result from two numerical experiments. However, they do prove that MR → RR transition is sensitive to rotation centre and initial condition.

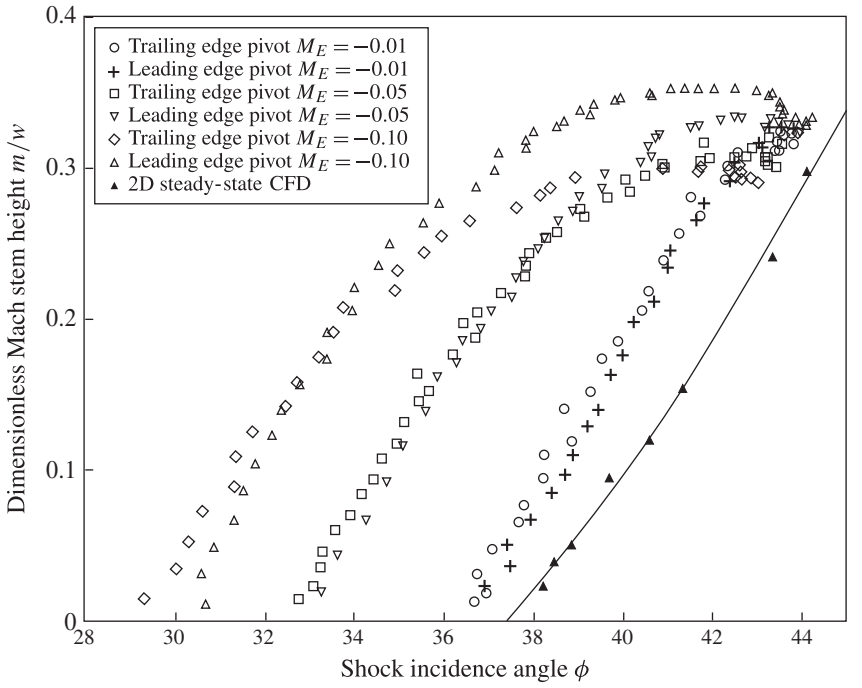

FIGURE 16. Computed variation of m/w with ϕ for rapid, impulsive rotation about the wedge leading and trailing edges with fixed $h/w = 1.01$ (for rotation about the leading edge) and fixed $g/w = 0.6$ (for rotation about the trailing edge). In all cases plotted here, $\theta_{wi} = 24.5°$, $M = 2.98$.

Case description	$\delta\theta_{WT}$	$\delta\phi_T$
$\theta_{wi} = 24.5°$, trailing edge pivot	10.4	10.9
$\theta_{wi} = 24.5°$, model pivot in experiment	12.0	9.4
$\theta_{wi} = 23.5°$, trailing edge pivot	10.2	9.1

TABLE 9. Sensitivity of $\delta\theta_{WT}$ and $\delta\phi_T$ to pivot point and θ_{wi} for $M_E = -0.1$ at $M = 2.98$.

5. Conclusions

Experiments were conducted to investigate dynamic MR → RR transition using a specially designed rig. Rapid wedge rotation generated a measurable effect on MR → RR transition. In experiments and computations for dynamic MR → RR transition at $M = 3.26$, transition was delayed approximately 0.8° below the corrected von Neumann condition. There was good agreement between experiment and CFD of the experiment. CFD was used to further investigate the sensitivity of transition to rotation speed, initial incidence and rotation centre in the strong and weak-reflection ranges. Owing to impulsive wedge start and rapid wedge rotation, there are very marked dynamic effects on the variation of Mach stem height with wedge incidence and the deviation from the steady transition conditions is significant. The MR → RR transition depends on the initial condition and the transient variation of Mach stem height with wedge incidence. For the range of rotation speeds investigated at $M = 1.93$ and 2.98, $\delta\phi_T$ ranged from 1.2° at $M_E = -0.01$ to 10.9° at $M_E = -0.1$. It was demonstrated that

MR can be maintained until zero wedge incidence with a sufficiently large rotation rate ($M_E = -0.1$ at $M = 1.93$). The dependence of transition to initial incidence and rotation centre is marked, especially at larger rotation speeds.

Acknowledgements

We would like to acknowledge the support of South Africa's Council for Scientific and Industrial Research, its Defence, Peace, Safety and Security Unit, the South African Department of Science and Technology, and the South African National Research Foundation.

REFERENCES

BEN-DOR, G. 2007 *Shock Wave Reflection Phenomena*. Springer.

FELTHUN, L. T. & SKEWS, B. W. 2004 Dynamic shock wave reflection. *AIAA J.* **42**, 1633–1639.

IVANOV, M. S., VANDROMME, D., FOMIN, V. M., KUDRYAVTSEV, A. N., HADJADJ, A. & KHOTYANOVSKY, D. V. 2001 Transition between regular and Mach reflection of shock waves: new numerical and experimental results. *Shock Waves* **407**, 85–104.

NAIDOO, K. & SKEWS, B. W. 2011 Dynamic effects on the transition between two-dimensional regular and Mach reflection of shock waves in an ideal, steady supersonic free stream. *J. Fluid Mech.* **676**, 432–460.

NAIDOO, K. & SKEWS, B. W. 2013 Consideration of the effect of length-scale information on regular to Mach reflection transition in the presence of dynamic effects. In *Twenty-Ninth International Symposium on Shock Waves. University of Wisconsin, Madison, USA*.

SKEWS, B. W. 2000 Three-dimensional effects in wind tunnel studies of shock wave reflection. *J. Fluid Mech.* **407**, 85–104.